7

Study of Michel Electrons in ProtoDUNE–SP

Contents

Studying electrons in the tens of MeV energy range can provide valuable input into reconstruction techniques and energy uncertainty for the measurement of astrophysical neutrinos from supernova bursts. Understanding the response of LArTPC detectors to electrons in this range will be important for any large scale LArTPC experiment wishing to study supernova bursts. At these energies electron interactions have large contributions from both ionisation energy loss and radiative energy loss and therefore they have a unique signature which is neither track–like or shower–like. Low–energy electrons therefore require unique reconstruction algorithms, to maximise the overall reconstruction performance.

This chapter will discuss an approach to low–energy electron reconstruction in LArTPC detectors based on the use of convolutional neural networks and semantic

segmentation. Michel electron events from ProtoDUNE–SP will be used to test the performance of this technique and to provide an estimate of the energy uncertainty of LArTPC detectors for low–energy electrons.

In this chapter Section 7.1 will discuss the signature left by Michel electrons in liquid argon, and the implications of this signature on reconstructing Michel electron events in ProtoDUNE–SP. This will be followed by a discussion of the algorithm used to select Michel electron events in Section 7.2. The Michel electron event reconstruction will be discussed in Sections 7.3. Finally, the results of this chapter and the implications for the DUNE far detector will be summarised in Section 7.4.

7.1 Michel Electrons in Liquid Argon

Michel electrons are produced when a muon decays at rest. In vacuum, this decay gives rise to a characteristic energy spectrum which has a sharp cut–off at around 50 MeV, corresponding to half the muon mass. In matter it is also possible for μ^- to be captured on nuclei before they decay, this causes a broadening of the Michel electron spectrum for these events. A comparison of the Michel electron energy spectrum for free μ^+ and captured μ^- is given in Figure 7.1. The capture process occurs roughly 70% of the time for negative muons in liquid argon, therefore, in ProtoDUNE–SP the observed Michel electron energy spectrum is a combination of the two processes in roughly equal quantities.

As discussed in chapter 4, the energy loss for electrons in liquid argon passes from an ionisation dominated regime to a radiation dominated regime in the tens of MeV region. The crossover point for this transition occurs at around 45 MeV, very close to the peak of the Michel electron spectrum. This leads to a unique signature for Michel electrons in liquid argon detectors, a short ($\sim$ 5cm) track segment is surrounded by a number of small radiated energy deposits. Figure 7.2 shows an example of a Michel electron candidate from ProtoDUNE–SP data, along with labels of the key features.

One of the main challenges for Michel electron reconstruction in liquid argon is to successfully associate the radiated energy depositions back to the initial

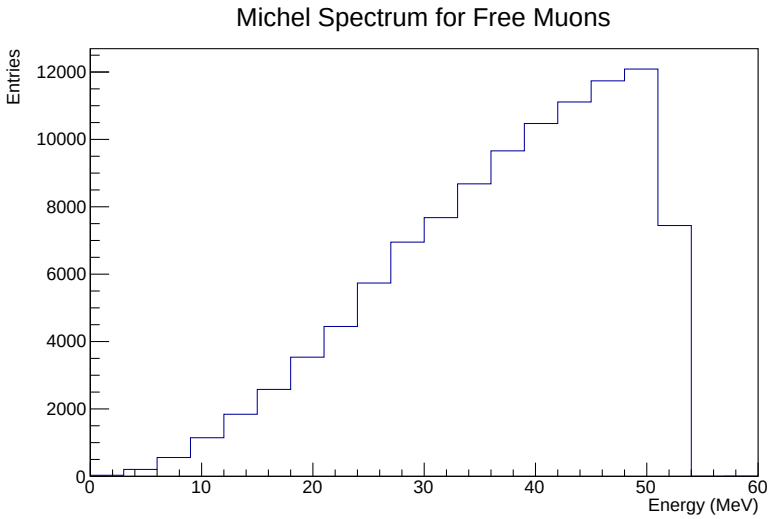

(a) Free Muons.

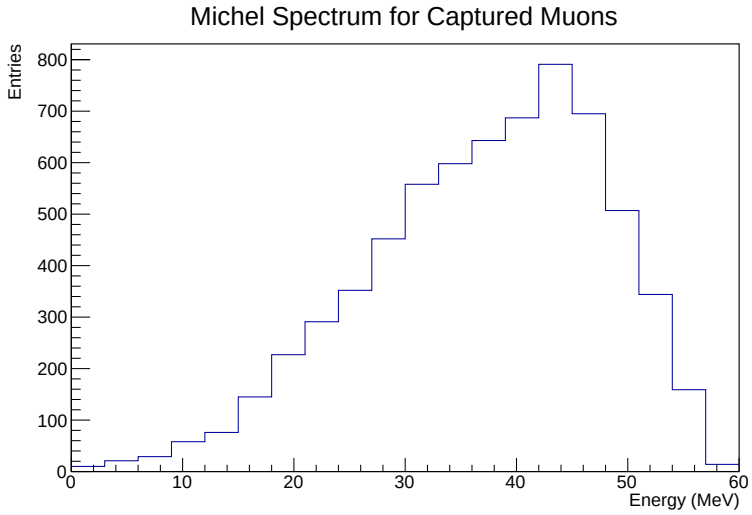

(b) Captured Muons.

Figure 7.1: Michel electron energy spectra in liquid argon from ProtoDUNE–SP simulation.

Michel electron once they have produced ionisation in the detector. Photons have a radiation length of around 20–30 cm in liquid argon which is many times larger than the size of the typical track–like part of the event, around 5 cm. Figure 7.3a shows the spectrum of radiated photons from Michel electron events in ProtoDUNE–SP simulation alongside the photon multiplicity as a function of Michel electron energy. While most of the radiated photons only carry a small fraction of the Michel electrons energy, in some cases a single radiated photon can carry a significant

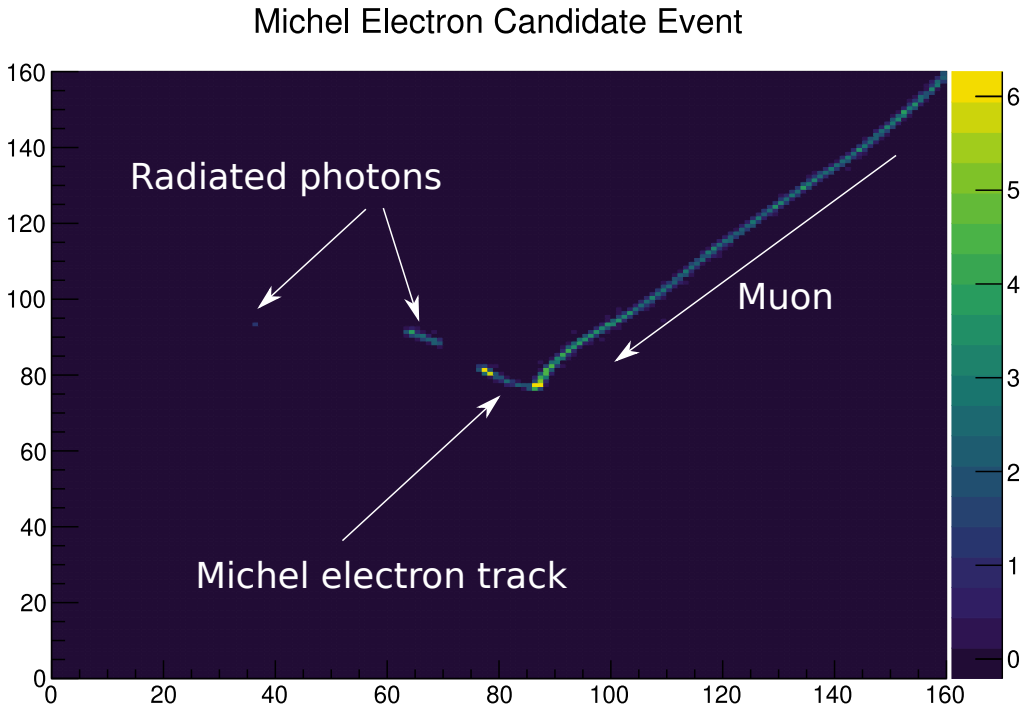

Figure 7.2: Michel electron candidate event from ProtoDUNE–SP data. The wire vs time data in the region of the Michel electron event is shown. The incoming muon, initial Michel electron track, and energy depositions from radiated photons have been labelled.

fraction of the electron energy. In addition, around the peak of the Michel electron spectrum ($\sim$ 45 MeV) there is a high photon multiplicity and a large spread in the multiplicity distribution. The combination of these effects leads to a significant spread in the fraction of radiated energy for Michel electron events.

The energy which is lost into radiated photons is only visible once the photons interact in the argon to produce secondary electrons which then ionise the argon. These secondary electrons are scattered over large angles and distances in the detector when compared to the short Michel electron track, the spatial distribution of secondary electrons is shown in Figure 7.4. This shows that the radiated energy deposits are spread over a large area, when compared to the size of the initial Michel electron track. Therefore, any reconstruction algorithm hoping to recover the radiated energy, will need to use data from a relatively large volume in order to maximise energy recovery.

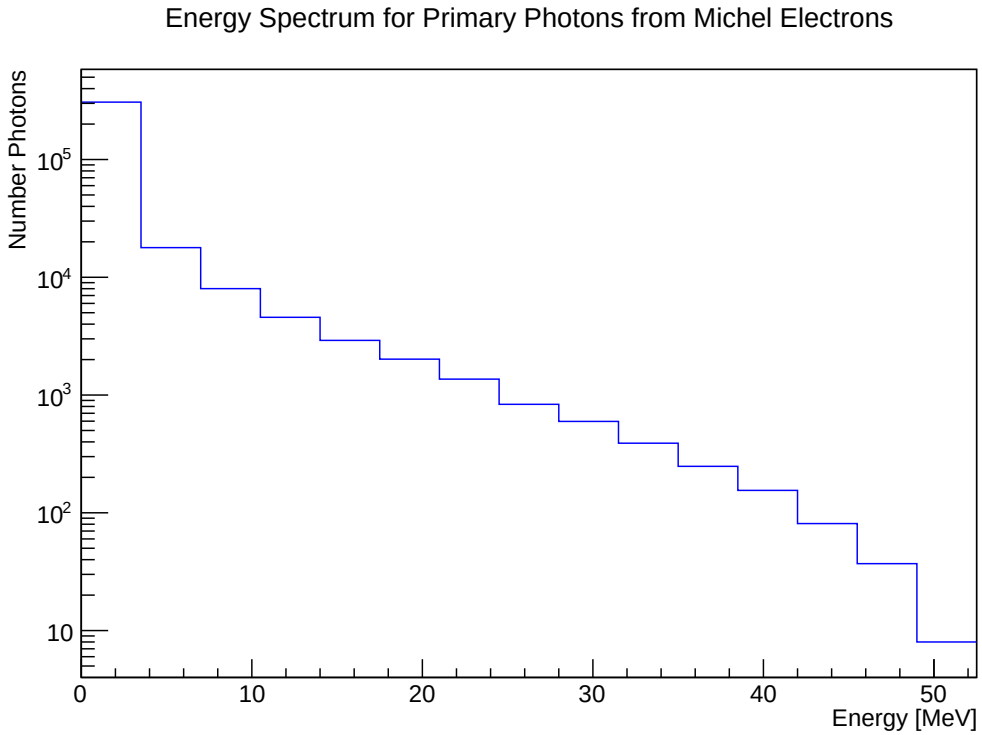

(a) Energy spectrum of radiated photons from Michel electron events.

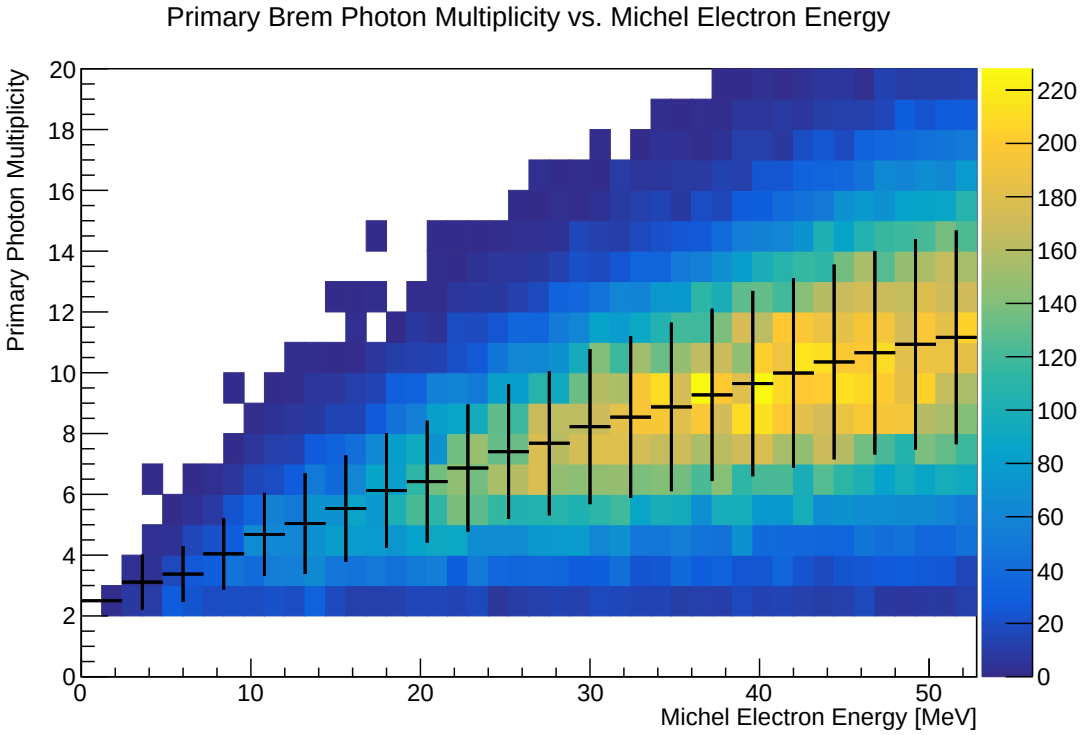

(b) Photon multiplicity as a function of true Michel electron energy. The distribution is overlaid with a profile of the mean of the distribution, the error bars on the profile represent the width of the distribution.

Figure 7.3: Properties of radiated energy deposits from Michel electrons in ProtoDUNE–SP simulation.

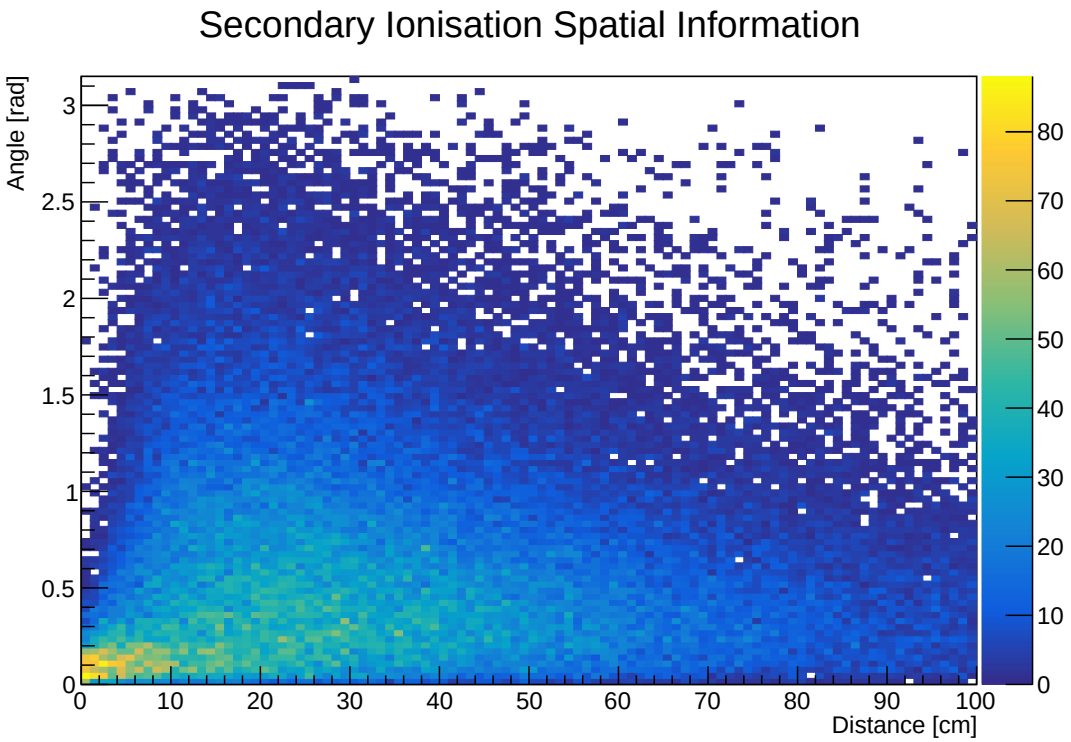

Figure 7.4: Spatial distribution of radiated ionisation deposits. This plot shows a 2D histogram of the distance and angle of each radiated energy deposition from the primary Michel electron track.

To highlight the impact of the radiated energy deposits we can consider the results of perfect energy reconstruction in two cases:

- Only considering the Michel electron track.
- Considering all ionisation energy within some radius and angle of the Michel electron track.

Figure 7.5 illustrates the considerable increase in energy collected if radiated energy is considered. The distribution is significantly narrower and much more energy is recovered when considering the energy deposited within a sphere of height 40 cm and angle 30°of the Michel electron vertex. In addition, the fraction of energy recovered as a function of Michel electron energy has a more linear distribution for a collection radius of 40 cm.

The average fractional energy recovery as a function of collection radius is shown in Figure 7.6, where the error bars represent the RMS of the distribution. By

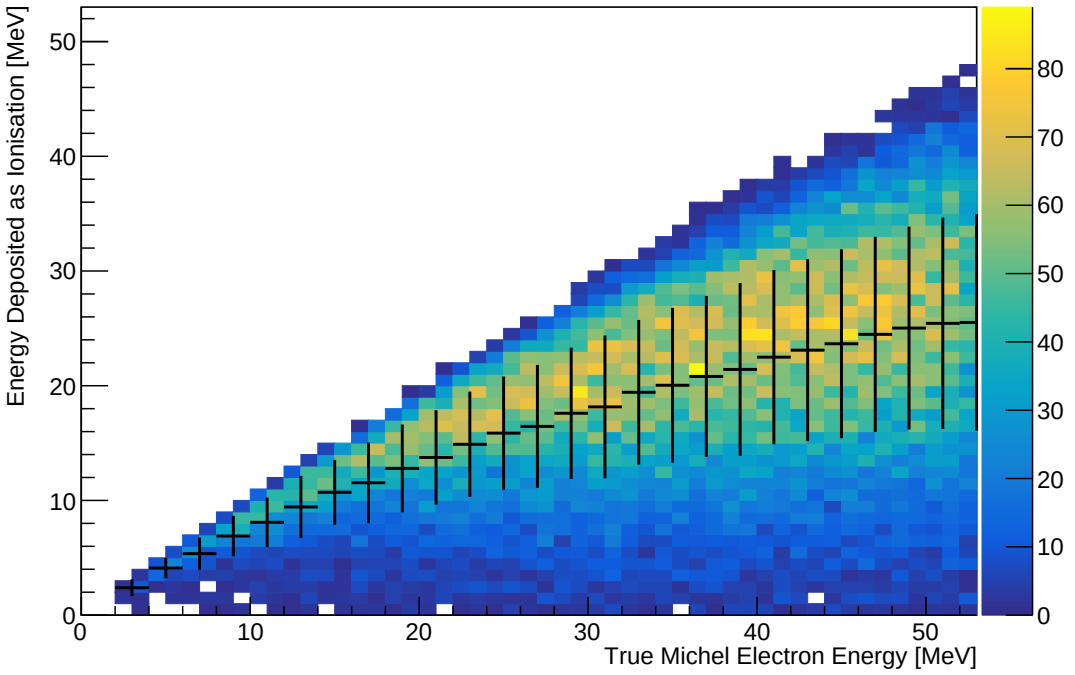

(a) True collected ionisation energy from the initial Michel electron track only.

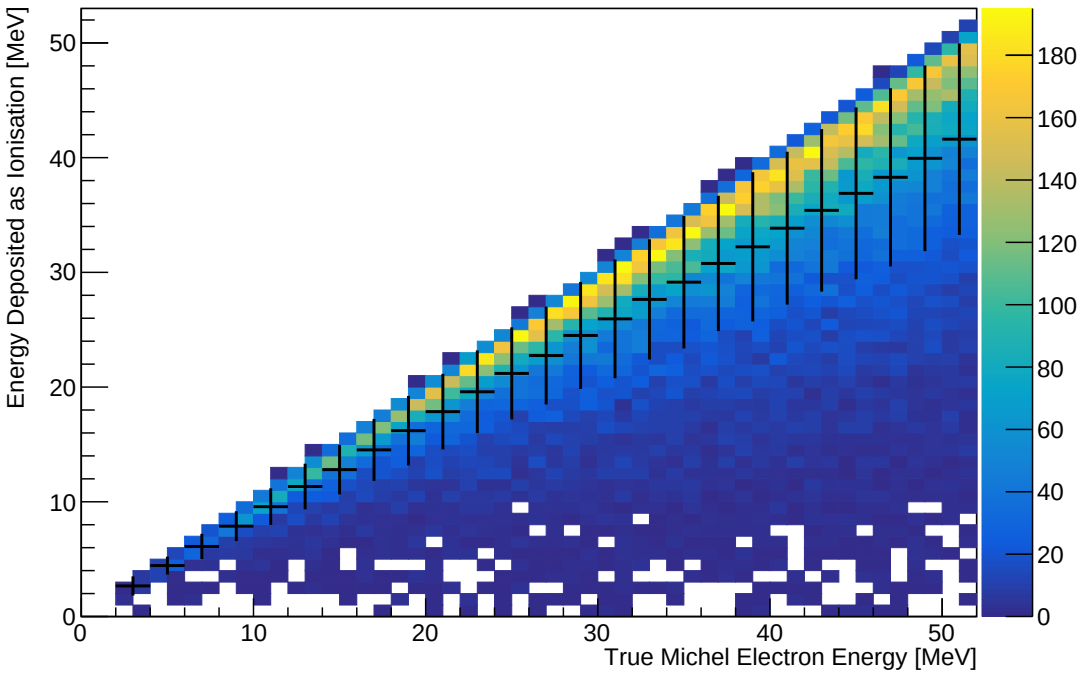

(b) True collected ionisation energy from the initial Michel electron track, and any radiated ionisation within a 40 cm cone at a 30° opening angle of the initial Michel electron track.

Figure 7.5: 2D histograms of the true collected ionisation energy vs the true Michel electron energy in ProtoDUNE–SP simulation.

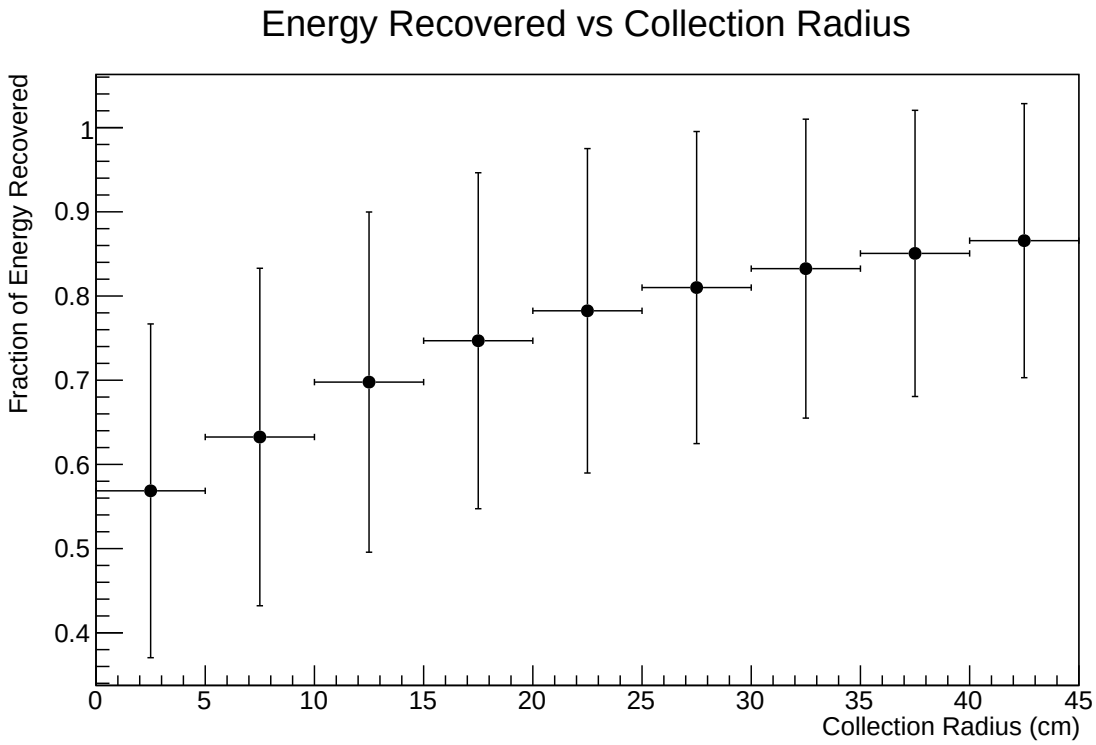

Figure 7.6: Fraction of Michel electron energy collected as ionisation vs collection radius.

increasing the collection radius from 0 cm to 40cm, the average energy recovered is increased from 57% to 87%. The RMS of the fractional energy recovered reduces slightly from 20% to 16% across this range. Therefore, the spread in the fraction of energy recovered is reduced from 35% to 18%.

Increasing the collection radius beyond around 30–40 cm gives minimal improvement in the fractional energy recovery from ionisation. This can been seen in Figure 7.7, which shows the total true ionisation energy collected for the case of a 40 cm collection radius and an 80 cm collection radius. While increasing the collection radius does not significantly increase the collected ionisation, it is likely to impact the purity and efficiency of reconstruction algorithms. Therefore, the energy reconstruction algorithm discussed in this chapter considers a 40 cm collection radius when collecting radiated energy deposits.

The MC study presented here highlights the importance of radiated energy deposits in Michel electron and other low–energy electron events. Based on these results it is clear that to minimise energy uncertainties for these events it is important

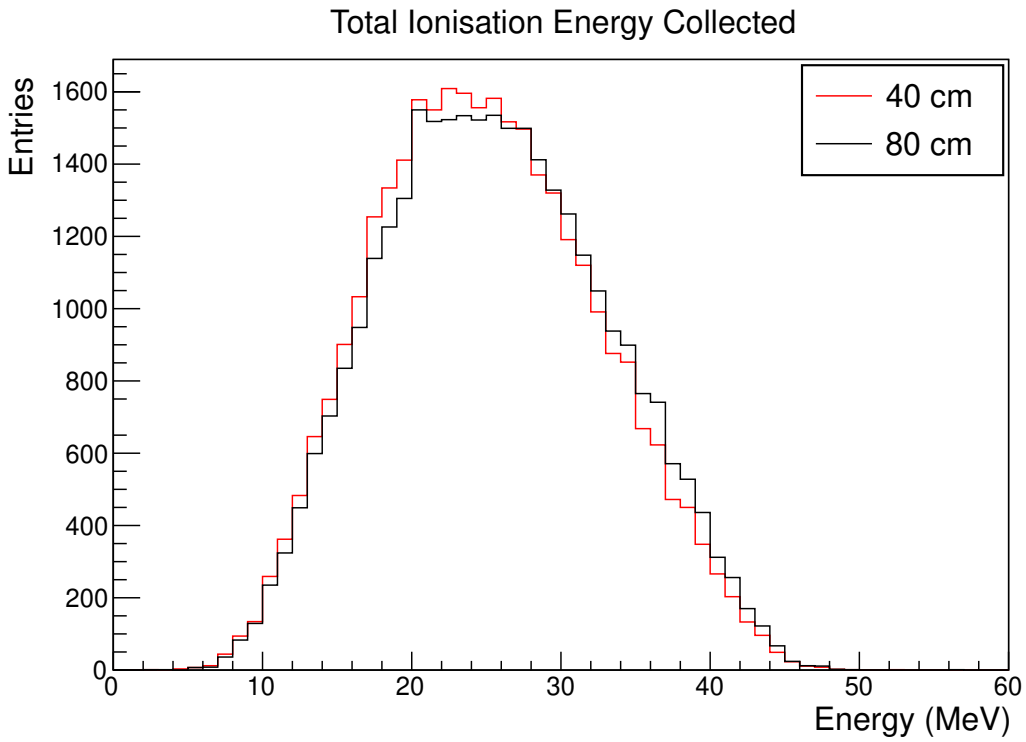

Figure 7.7: Total true ionisation energy recovered for a 40 cm collection radius, and an 80 cm collection radius.

to maximise the amount of energy collected from radiated photons. The rest of this chapter will discuss an algorithm which was developed to tackle this problem, and it's application on Michel electron events in ProtoDUNE–SP data.

7.2 Michel Electron Event Selection

In order to select Michel electrons in ProtoDUNE–SP data, an event selection algorithm was developed based on combining the results from the hit tagging CNN from the previous chapter with clustering performed by the main ProtoDUNE–SP reconstruction framework, Pandora.

The event selection algorithm has four steps:

1. Start with all primary tracks from Pandora.

2. Define a set of Michel electron candidates from the list of all daughters of the track.

3. Find the best Michel electron candidate from the list of Michel electron candidates.

4. Select events where the best Michel electron candidate passes the event selection cuts.

First, the initial sample of muon candidates is defined. All tracks from the Pandora reconstruction chain which have been labelled as primary tracks are considered.

The second step defines a set of Michel electron candidates for each muon candidate. A Michel electron candidate is any daughter of the primary Pandora track which satisfies the following conditions:

- Starts within 5 cm of the primary track endpoint.
- Contains a minimum of 5 reconstructed hits on the collection plane.

In the third step, the Michel electron candidates are analysed in order to define the best Michel electron candidate for each muon candidate. The best Michel electron candidate is the Michel electron candidate with the largest fraction of Michel–like hits based on the output of the Michel electron score from the CNN. A threshold of 0.9 is used to identify hits as Michel–like. In the case of a tie the Michel electron candidate with the most hits is chosen.

The fourth step is the final decision, which is based on the fraction of Michel like hits in the best Michel electron candidate. Events are selected if the best Michel electron candidate is made up of more than 80 % of Michel–like hits. Figure 7.8 shows a comparison of the fraction of Michel–like hits in Michel electron candidates for ProtoDUNE–SP data and simulation. There is a good agreement between data and simulation. The pile–up of events at one corresponds to Michel electron candidates where all hits were classified as Michel–like.

Based on this algorithm Michel electron events are selected with a purity of 98% and an overall efficiency of 6% in ProtoDUNE–SP simulation. Figure 7.9 shows the event selection efficiency as a function on Michel electron energy. The efficiency is reasonably consistent across the energy range, however, there is a significant

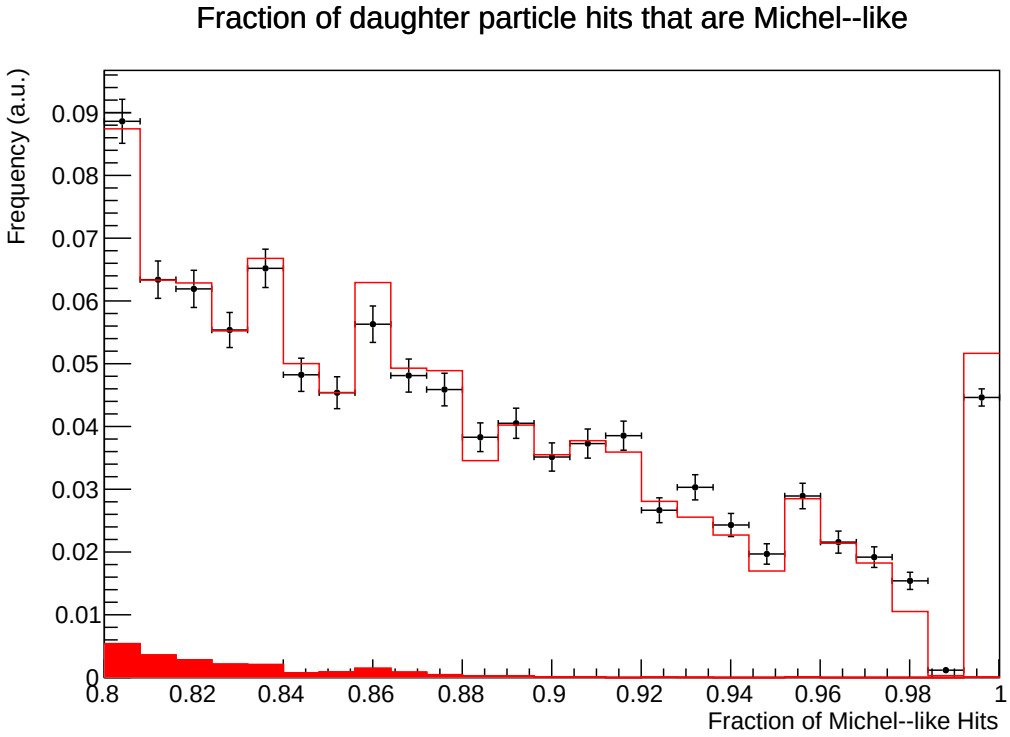

Figure 7.8: Fraction of Michel–like hits in the best Michel electron candidate in data and simulation. The red line is the total distribution in simulation, and the solid red region represents the predicted background in simulation. The black distribution is the results in data, where the error bars are statistical only.

reduction for energies below 5 MeV. The efficiency is highest for Michel electrons in the range of 10–40 MeV, and reduces slightly at high energies. At 40–50 MeV, around the peak of the Michel electron spectrum, the efficiency is around 5%.

To accurately estimate the energy of hits during energy reconstruction, the true time of the Michel electron needs to be known. If the true time is not known, then the drift time of the charge is unknown, and the charge attenuation cannot be estimated. Therefore, only tracks with reconstructed true times were considered for the Michel electron analysis. The spatial and angular distributions of the primary muons, normalised by the number of selected muons, are shown in Figure 7.10. There is a reasonable agreement between data and simulation for both the spatial and angular distributions of the primary muons.

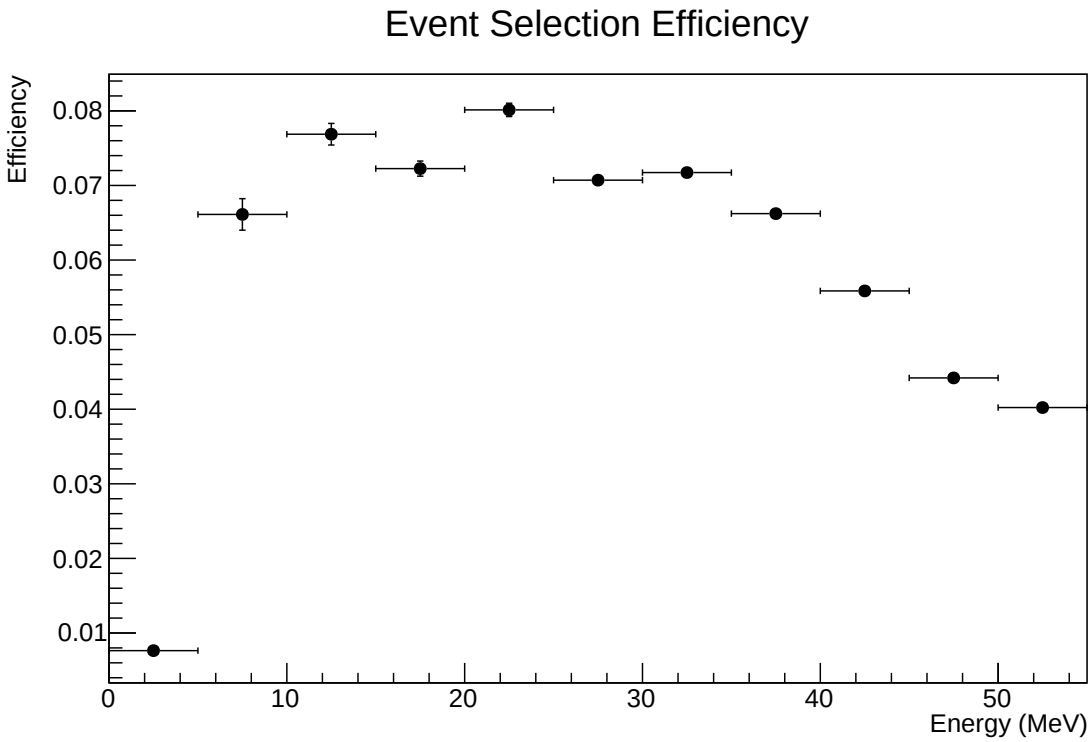

Figure 7.9: Efficiency of Michel electron event selection as a function of true Michel electron energy in ProtoDUNE–SP simulation.

7.3 Michel Electron Energy Reconstruction

To reconstruct the energy of Michel electrons in liquid argon the relevant hits must first be selected. Once the hits are selected the ionisation energy deposited by each hit is then reconstructed, the reconstructed energy of the Michel electron is the sum of the reconstructed energy of all relevant hits. In this section we will detail a hit selection algorithm based on a type of convolutional neural network called a U-Net, which returns hit selection maps for the Michel electron energy reconstruction. This algorithm is used to select Michel electron hits with a high purity and efficiency, the resulting reconstructed energy spectrum is used to estimate the energy resolution of ProtoDUNE–SP for electrons in the tens of MeV range.

7.3.1 Michel Electron Hit Tagging with U-Nets

A U-Net is a type of convolutional neural network which is designed to perform semantic segmentation of images, which was first developed for biomedical image

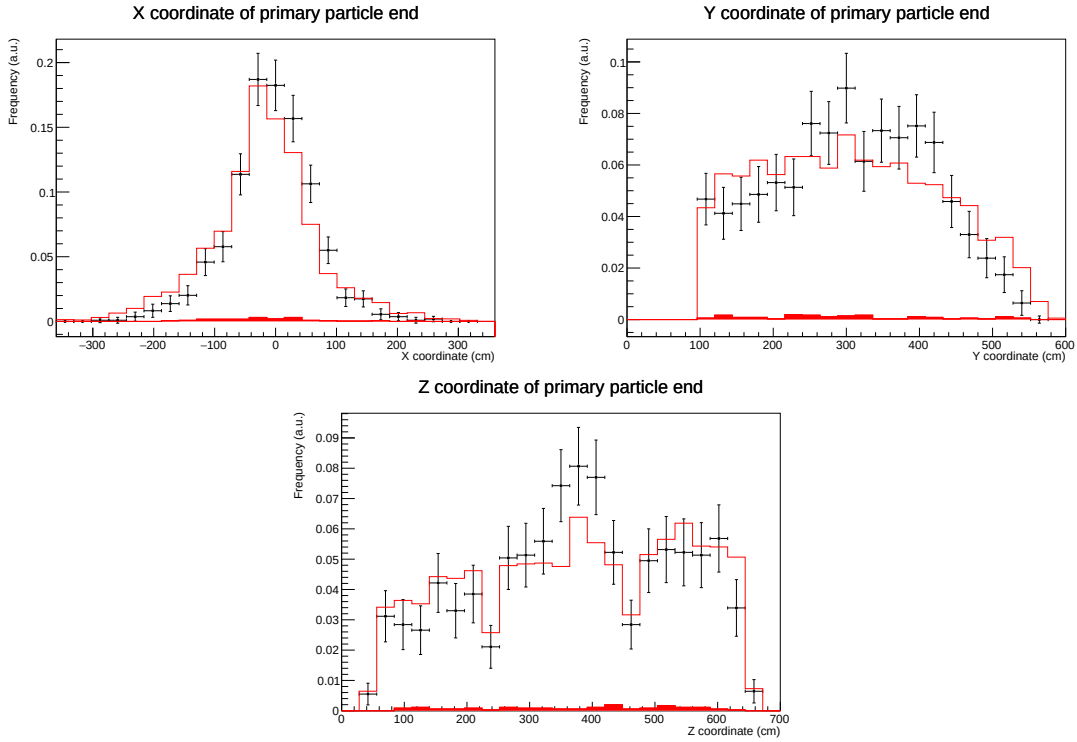

(a) Primary muon end–points.

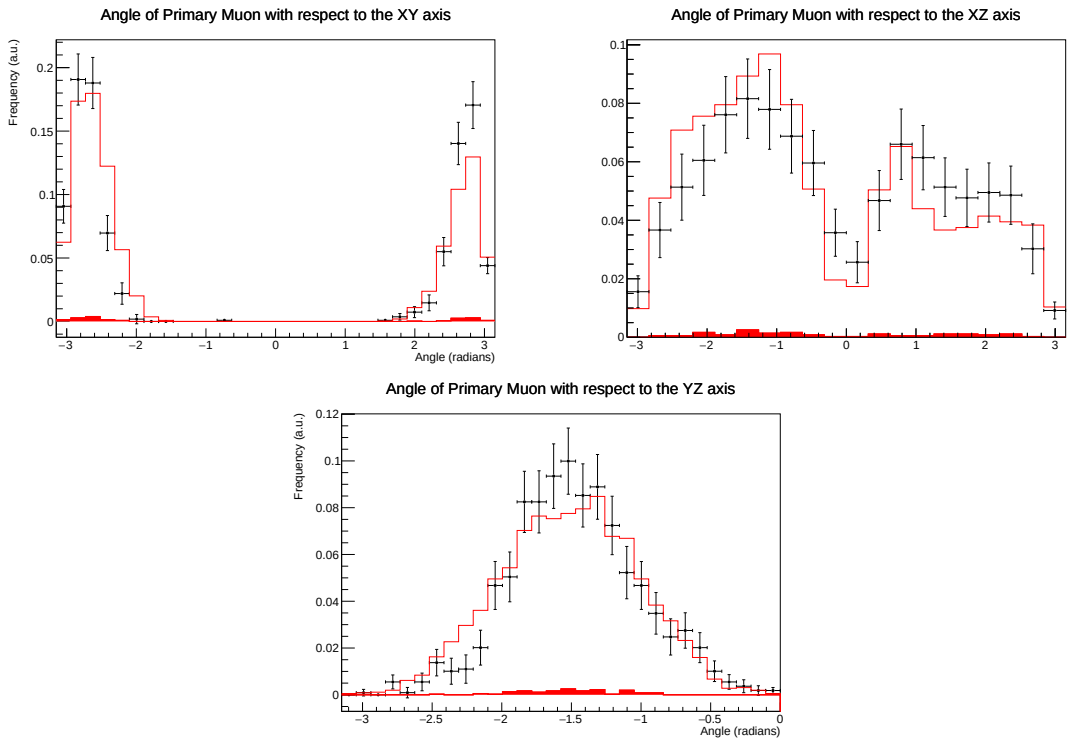

(b) Primary muon angular distributions.

Figure 7.10: Spatial and angular distributions for primary muons associated with selected Michel electrons.

segmentation[120]. In semantic segmentation the goal is to return a map of pixels which correspond to the areas of interest; the output of the network is the same dimension as the input with a one–to–one correspondence between input pixels and output pixels. The architecture used for the hit selection algorithm is shown in Figure 7.11. During the first half of the network architecture the resolution of the output is decreases, this is analogous to many conventional CNN's and during this phase the network learns about the content of the image. The second phase of the architecture allows the U-Net to rebuild the locations of different features within the initial image, this is achieved by passing the details of previous layers to the network as the resolution of the output map is slowly increased back to the original resolution.

In the Michel electron case, the goal of the network is to return a map of all ionisation energy deposits which come from the Michel electron, this includes the initial track and any secondary deposits from radiated photons. The inputs and outputs are two dimensional images of the location of reconstructed hits centered on the selected Michel electron. The amplitude of each input pixel is given by the integrated charge of any reconstructed hits within the pixel. For the outputs the pixels have an amplitude of 1 if they contain a Michel electron hit, and 0 otherwise. Only data from the collection plane is used because there is a higher signal to noise ratio on these wires.

The F_β metric was used as the loss function for the U–Net. This loss is a generalised version of the F_1 metric discussed in Chapter 6, which allows for the relative importance of precision and recall to be tuned,

$$F_\beta = \left(1 + \beta^2\right) \frac{precision \cdot recall}{(\beta^2 \cdot precision) + recall}. \tag{7.1}$$

This loss rewards the network for selecting as many correct hits as possible (high recall), while penalising it for selecting more hits that necessary (low precision). The F_β score lies between 0 and 1, with a score of 1 corresponding to a perfect match. The $\beta parameter was chosen to be 2, such that recall was considered to be more important than precision. This w$ was performed.

The network architecture used for the Michel electron reconstruction is shown in Figure 7.11. The network consists of a repeating structure which contains the following key components:

- Convolutional blocks, which contain multiple convolutional layers.
- Pooling layers for downscaling in the first half of the network.
- Residual connections and up–sampling in the second half of the network.

The convolutional blocks each contain three convolutional layers, which is shown in Figure 7.11b. These take the form of inception units[91] with Leaky ReLU activation functions, a schematic of the inception units is shown in Figure 7.11c. During the first half of the network, maximum pooling is used to downsample the size of the feature maps, which reduce by a factor of two in each max pooling layer. Then, during the second half of the network, the up–sampling layers increase the resolution of the feature maps by a factor of two, such that the output of the network has the same resolution as the input. The residual connections from early layers, are combined with the up–sampled feature maps, to allow the network to reconstruct the location of the learned features. As with the CNN from the previous chapter, both dropout and early–stopping are implemented to prevent over–fitting.

The datasets for the training process were generated from a full simulation of the ProtoDUNE–SP detector under beam operation including both cosmic–ray and beam particles. The images produced contain the location and integrated charge for each hit within the image window. The training data is split into training, test, and validation sets in the ratio 80:10:10. In total around 15,000 images used in the training, test, and validation datasets.

As with the hit tagging CNN from the previous chapter, the training and validation scores were monitored throughout training using TensorFlow. The weights of the network were saved after each epoch, and the final weights were those from the epoch before the epoch when the validation score first decreased. Figure 7.12 shows the evolution of the loss over time, along with a vertical line representing the loss at which the weights were chosen.

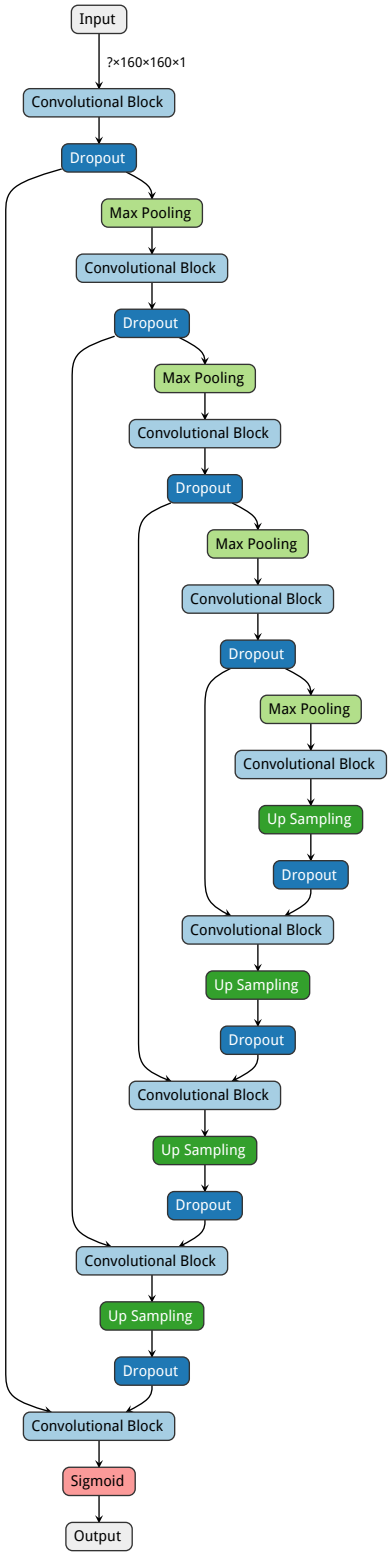

(a) Overall structure.

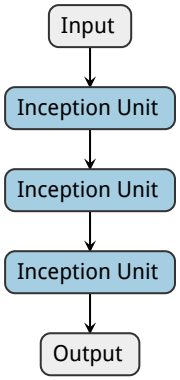

(b) Convolutional block.

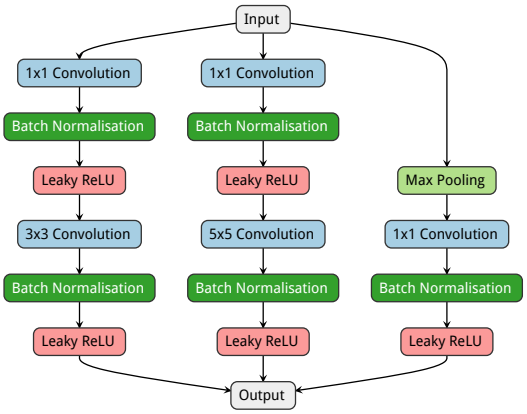

(c) Inception unit.

Figure 7.11: U–Net CNN architecture used to select ionisation energy deposits. Visualisation adapted from the output of the Netron neural network viewer[108].

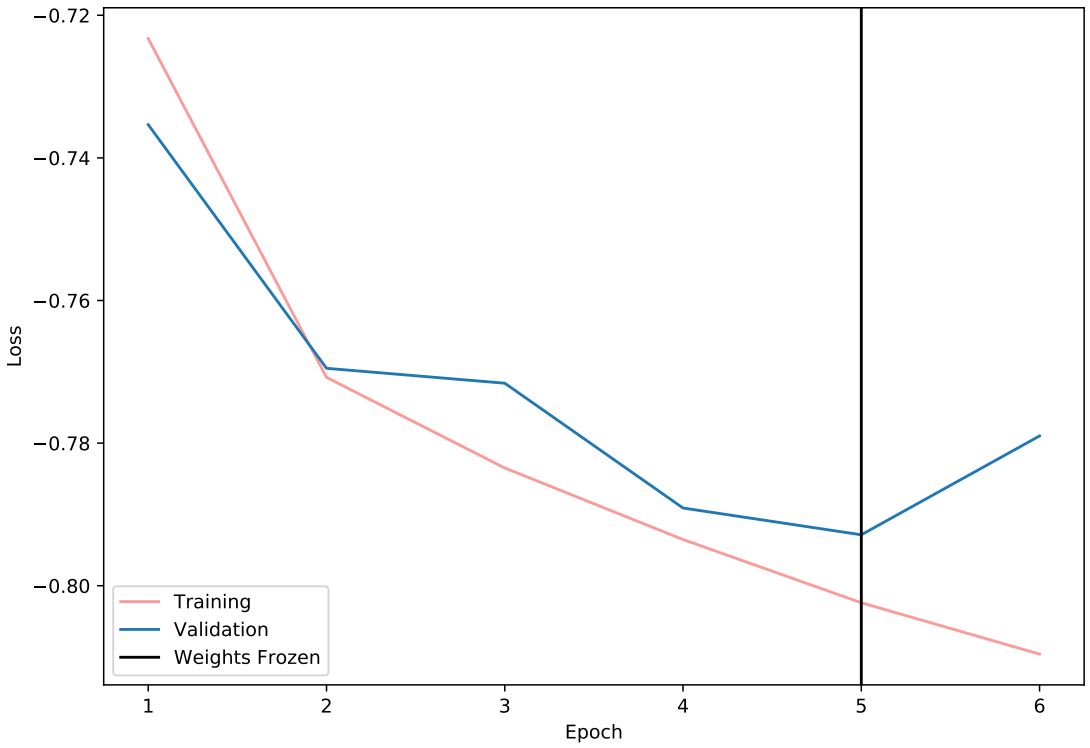

Figure 7.12: U-Net training and validation loss as a function of epoch. The weights were frozen based on an early stopping algorithm, which is demonstrated by the vertical black line.

A demonstration of the output of the U-Net is given in Figure 7.13 which shows the input, output, and truth images for an event from ProtoDUNE–SP simulation.

7.3.2 Michel Electron Reconstruction

Michel electron reconstruction was evaluated on a dataset which was part of the same batch of simulation as the training, test, and validation data, but distinct from all of them.

7.3.2.1 Hit Selection

The U-Net produces a sharply peaked output distribution in both data and simulation as seen in Figure 7.14, the histograms here are normalised by the number of entries. Both distributions show sharp peaks at zero and one, but the distribution has slightly sharper peaks in simulation, which can be seen because the data has a tendency to be above the simulation for scores far from zero and

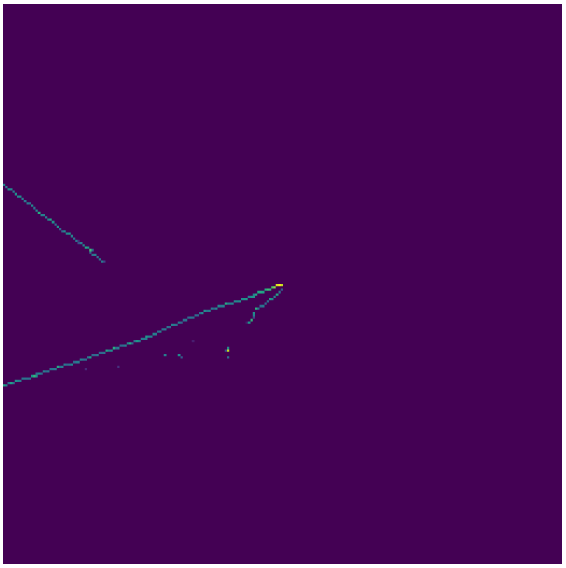

(a) Input.

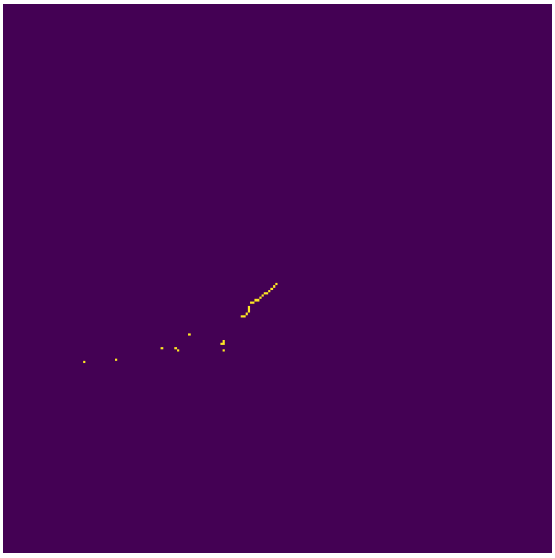

(b) Truth.

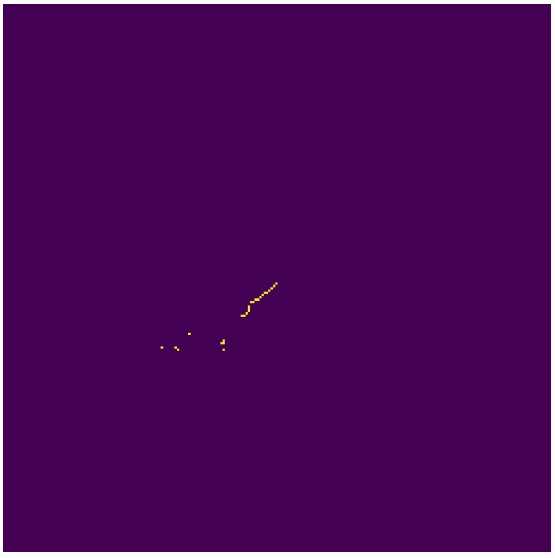

(c) Prediction.

Figure 7.13: Example input, truth, and prediction images for U-Net.

one. Hits from the input images are selected as Michel electron hits if their score exceed a selection threshold of 0.9. In simulation 7.8% of hits are selected, while in data the fraction selected is 8.0%, therefore, there is a 2.5% difference in the selected fraction between data and simulation.

The performance of the hit tagging algorithm was analysed with the simulated sample. Based on the score distributions for true and false hits the precision and completeness of the hit tagging algorithm can be evaluated. The precision

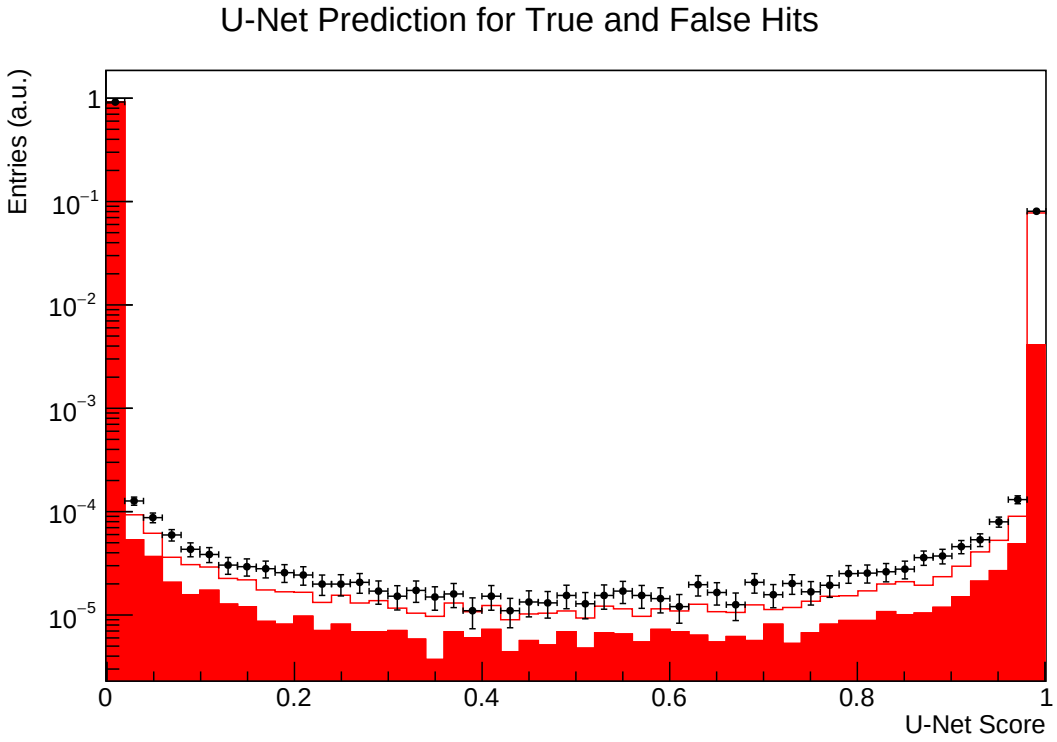

Figure 7.14: U–Net predicted distribution for hits in images. The simulated results are shown by the red line, with the backgrounds as a shaded red region. The data is shown in black, with statistical error bars.

and completeness are defined as

$$\text{Precision} = \frac{N_{TP}}{N_{TP} + N_{FP}} \tag{7.2}$$

$$\text{Completeness} = \frac{N_{TP}}{N_{TP} + N_{FN}} \tag{7.3}$$

where N_{TP}, N_{FP}, and N_{FN} are the number of true–positives, false–positives, and false–negatives respectively. These parameters give a quantitative evaluation of the performance of the hit tagging algorithm, allowing for comparison between different algorithms.

The purity and completeness of the hit tagging was calculated for a range of selection thresholds in the range $[10^{-7}, 1-10^{-7}]$, Figure 7.15 shows the purity against completeness for the values in this range. The hit tagging algorithm produces a high precision and completeness throughout the range of thresholds, however the steepness of the score distributions means that the choice of threshold makes little

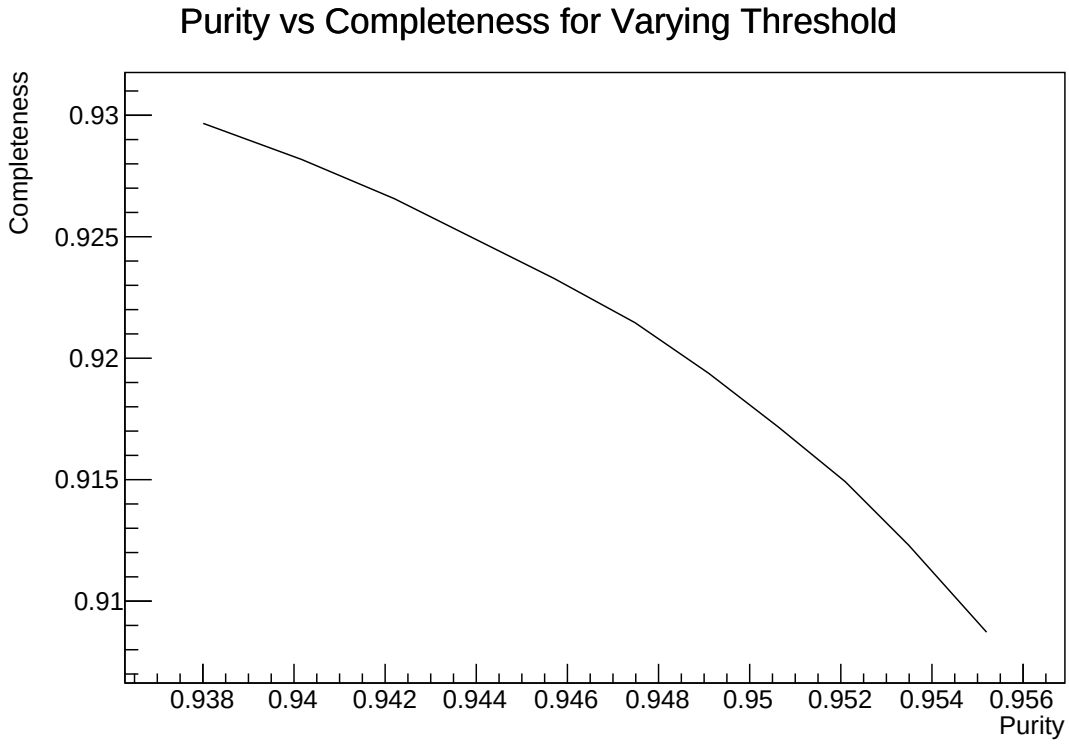

Figure 7.15: Hit tagging purity vs completeness for the U–Net algorithm on ProtoDUNE–SP simulation.

difference to the performance, meaning that little can be done to optimise the performance by varying the threshold.

The number of hits selected per event for data and simulation is shown in figure 7.16. Around 10 hits are selected on average per event, with a tail extending up to around 30 hits. The distribution of the backgrounds follows a similar distribution to the true events. A good agreement is seen between the data and simulation for the number of selected hits, these hits are then used to reconstruct the deposited ionisation energy of the Michel electron.

7.3.2.2 Ionisation Energy Reconstruction

The total ionisation energy is reconstructed by summing the hit–by–hit ionisation energy for all hits selected by the U-Net. The ionisation energy for each hit is reconstructed from the hit integral in ADC as

$$E_{hit} = \frac{I_{hit} \times C_X \times C_{YZ} \times N \times W_{ion}}{C \times R}, \tag{7.4}$$

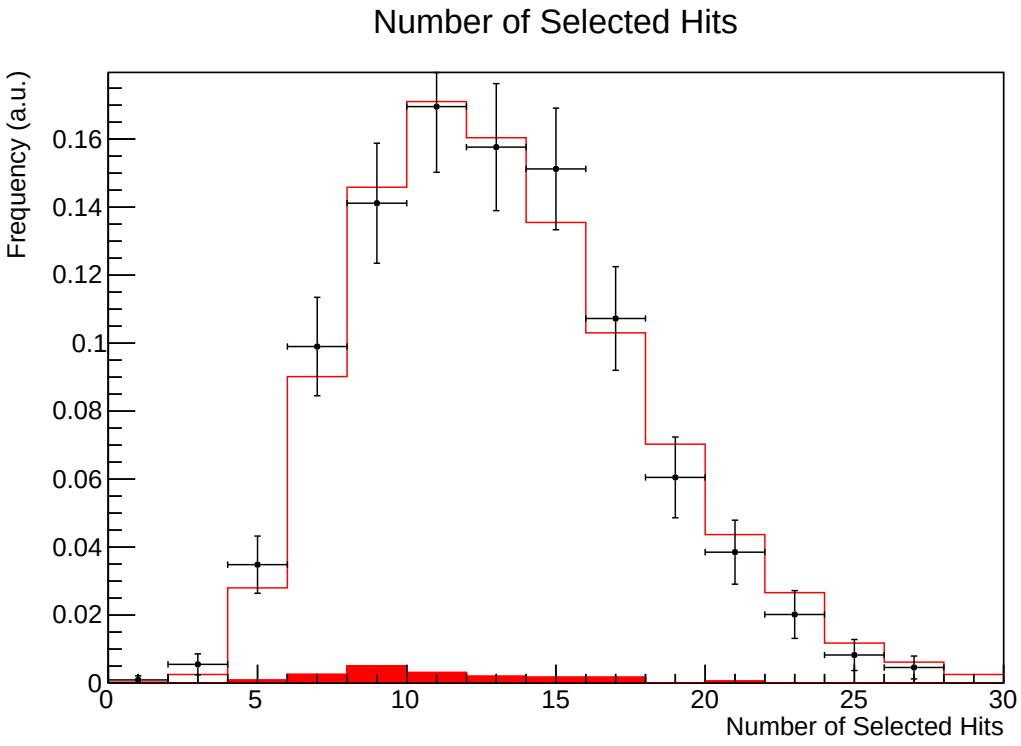

Figure 7.16: Number of hits selected by the U–Net for Michel electron candidate events in data and simulation.

where E_{hit} is the reconstructed hit energy in MeV, I_{hit} is the integrated hit charge in ADC, C_X is the X–correction factor which is dependent on the X coordinate of the hit within the TPC, C_{YZ} is the YZ–correction factor which is dependent on the Y and Z coordinates of the hit within the TPC, N is a dimensionless normalisation factor which normalises the data and MC distributions to give the same magnitude, W_{ion} is the ionisation energy of argon in MeV per electron, C is a constant conversion factor which has units ADC per electron, and R is the recombination factor. The distribution of reconstructed hit energies in ProtoDUNE–SP data and simulation is shown in Figure 7.17.

The position dependent calibration matrices correct for non-uniformity in the detector response across the TPC. In the X direction, which is parallel to the drift direction, the main contributing factors are attenuation due to electron absorption, and variations in the electron drift velocity due to space charge effects. The main contributing factor for the YZ–correction factor are wire–to–wire response variations.

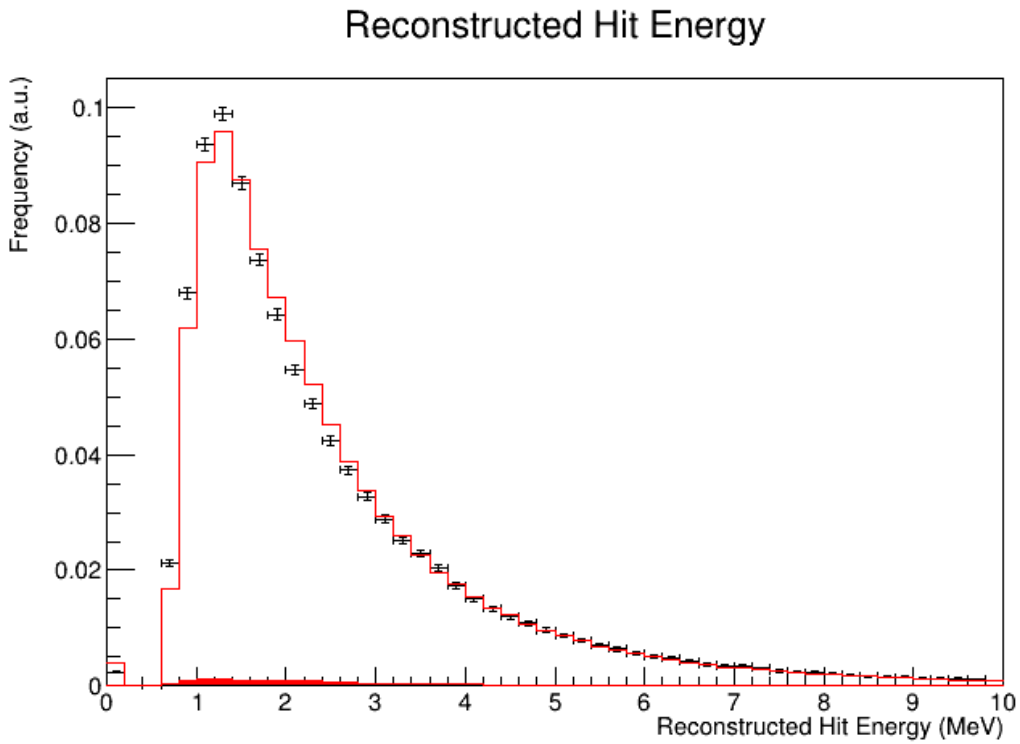

Figure 7.17: Reconstructed Hit Ionisation Energy for hits in Michel electron input images in data and simulation.

As discussed in chapter 4, the recombination factor is a dE/dx dependent factor, which depends on the conditions in the liquid argon. Due to the shortness of Michel electron tracks and the other charge deposits, it is challenging to assign dE/dx on a hit–by–hit basis for this sample. Therefore, an average recombination factor is used for all hits. The recombination factor was calculated using the box model [73] under ProtoDUNE–SP operating conditions, which gives an average value of 0.69.

As a result of the spatially dependent calibration factors, the energy of hits can only be accurately reconstructed for events with a reconstructed true time. This leads to a significant drop in event selection efficiency, which is due to the fact that only 15% of cosmic–ray tracks have a reconstructed true time in simulation and only 1% in data.

The reconstructed Michel electron energy is the sum of the reconstructed ionisation energy for all selected Michel electron hits. The reconstructed ionisation energy spectrum for Michel electrons in ProtoDUNE–SP is shown in Figure 7.18.

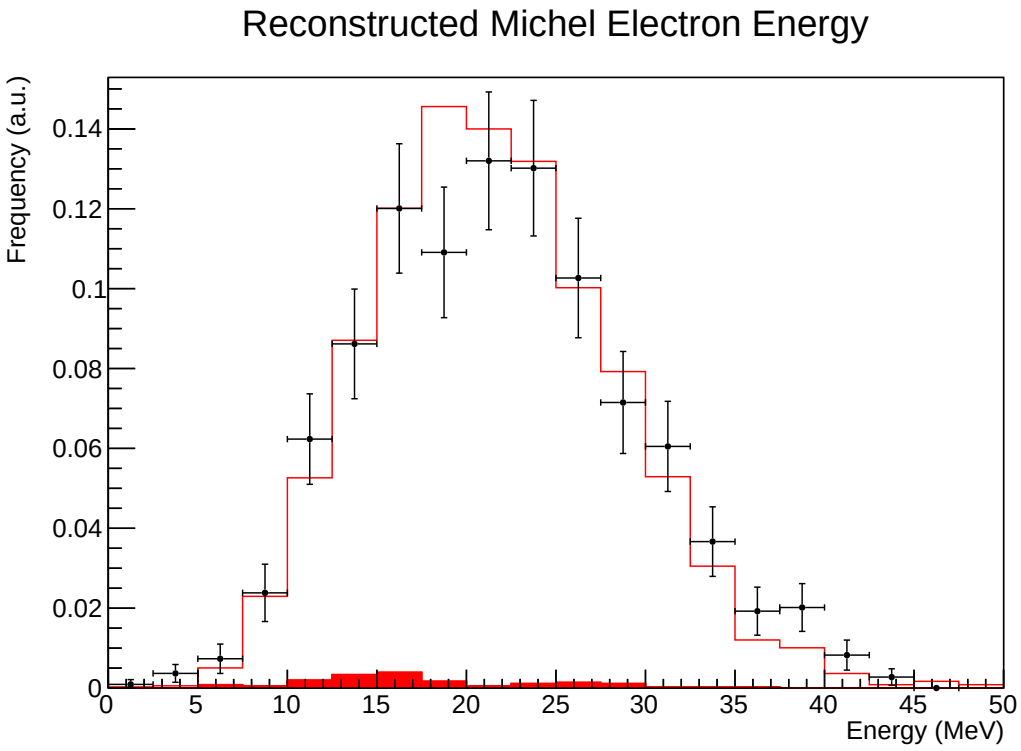

Figure 7.18: Reconstructed Michel electron ionisation energy in data and simulation.

The distribution peaks at around 20 MeV and has a tail up to just under 50 MeV, which is consistent with the true ionisation energy deposited by Michel electrons within a 40 cm radius, shown in Figure 7.7.

The performance of the ionisation energy reconstruction was evaluated with the simulated Michel electron sample. First, the reconstructed ionisation energy was compared to the true ionisation energy, and a linear scaling factor was calculated to correct for any energy offset. The correction factor was calculated based on a liner fit to the distribution of reconstructed energy against true energy, which is shown in Figure 7.19. The reconstructed energy was corrected based on this linear fit,

$$E_{corr} = \frac{E_{reco} - 0.808 \text{ MeV}}{0.9567},$$

and the corrected energy was used to estimate the energy resolution and bias of the Michel electron energy reconstruction.

To estimate the resolution and bias of the ionisation energy reconstruction, the fractional difference between the reconstructed and true ionisation energy was

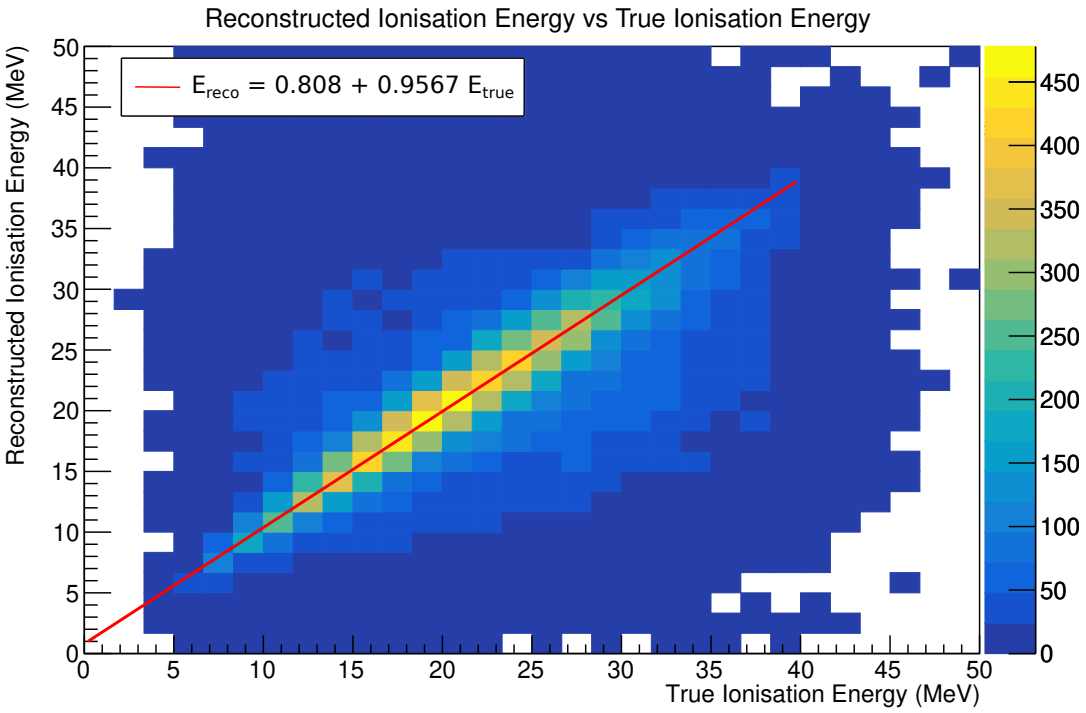

Figure 7.19: Reconstructed Ionisation vs True Ionisation.

considered. We define the fractional difference as,

$$\text{Fractional Difference} = \frac{E_{corr} - E_{true}}{E_{true}},$$

such that the spread of the distribution is a measure of the fractional uncertainty of the reconstructed energy. The energy resolution and bias were estimate by fitting a gaussian to the fractional difference distribution; the standard deviation of the gaussian was taken to be an estimate of the energy resolution, and the mean of the gaussian was taken to be an estimate of the bias. The distribution of the fractional difference for all events, and the associated gaussian fit, are shown in Figure 7.20. Based on this fit the energy resolution was estimated to be around 10% and the bias around 1%. However, it is worth noting that the fractional difference distribution has a fairly significant tail for negative fractional differences, and therefore the fit was restricted to the central region of the distribution.

Studies into the energy resolution and bias as a function of energy gave insights into the source of the tail in Figure 7.20. These were investigated by binning the

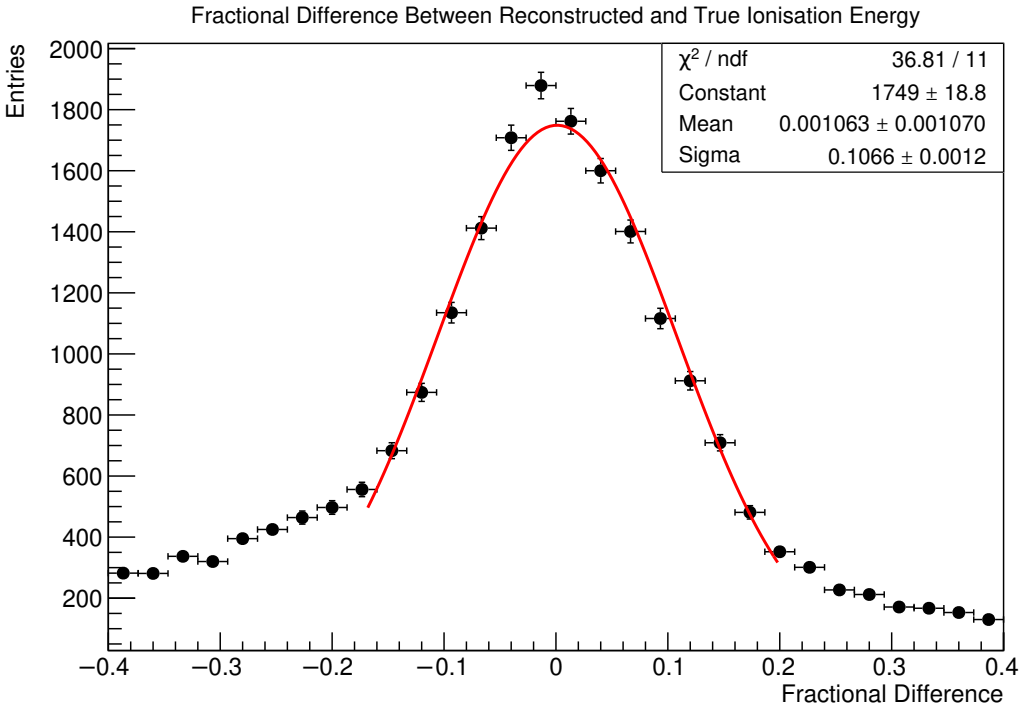

Figure 7.20: Fractional energy difference between reconstructed and true Michel electron energy.

fractional energy difference distribution in terms of true ionisation energy, and performing the same gaussian fit to the fractional difference distribution for each energy bin, to estimate the energy resolution and bias. The measured energy resolution and bias as a function of true ionisation energy are shown in Figure 7.21, the associated fits are given in Appendix A.

The energy resolution and bias as a function of energy demonstrates that the energy reconstruction algorithm is capable of good energy reconstruction performance. However, it is important to note that above around 25 MeV there is significant tail for negative fractional differences. This is due to a reduction in the hit tagging efficiency in the high energy region, which causes less of the initial Michel electron energy to be collected by the CNN. No attempt was made to fit this tail, and therefore the estimated energy resolution and bias based on the gaussian fits, used to populate Figure 7.21, overstate the performance in the high energy region. A more conservative estimate can be made by considering

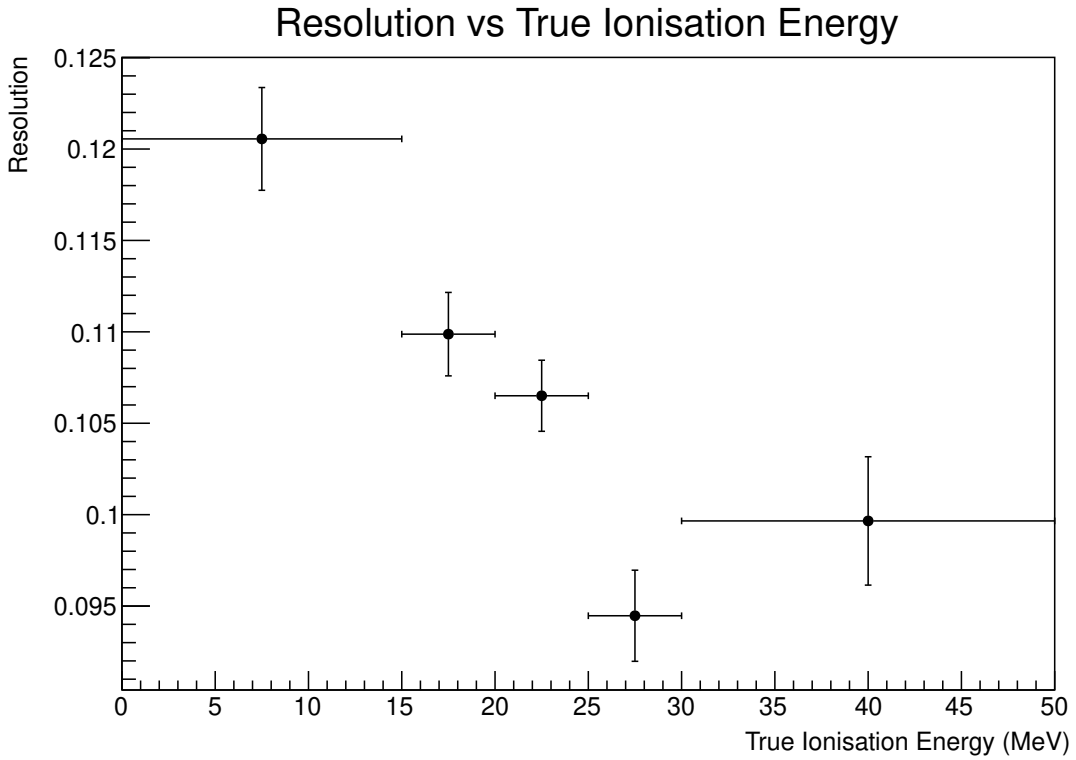

(a) Resolution.

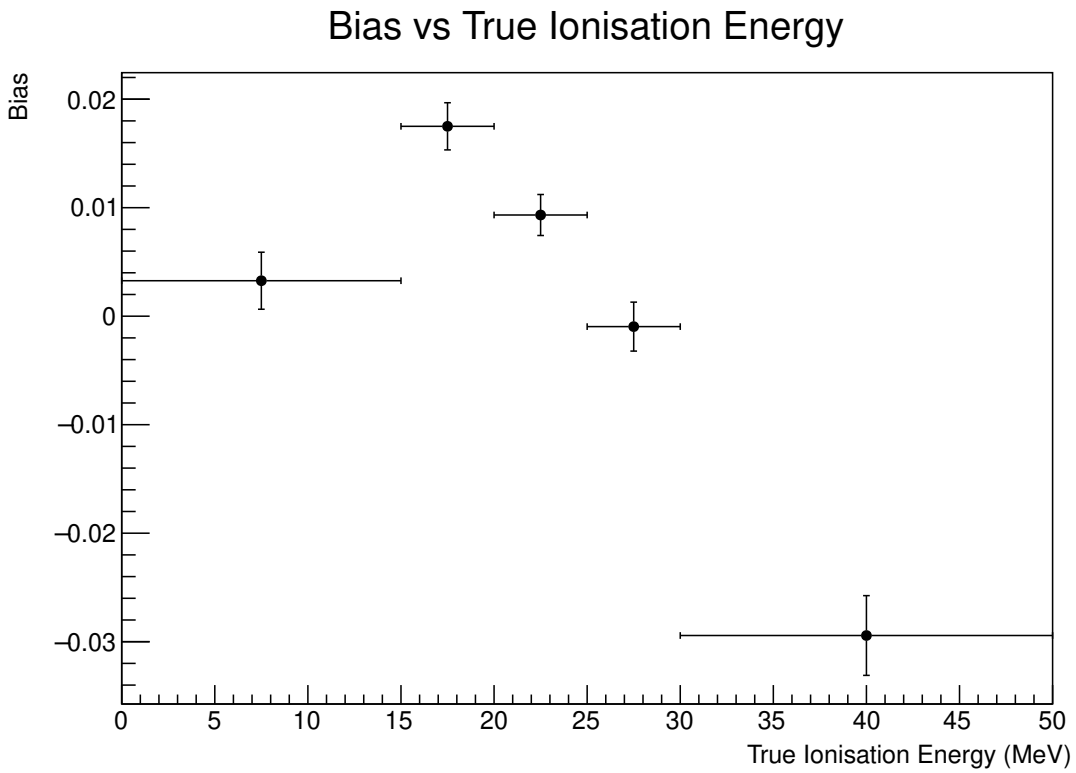

(b) Bias.

Figure 7.21: Energy resolution and bias as a function of true ionisation energy deposition.

Energy Bin	Gaussian Mean	Gaussian Sigma	Mean	RMS
0–15 MeV	0.0033	0.1206	0.0082	0.1501
15–20 MeV	0.0175	0.1099	0.0176	0.1472
20–25 MeV	0.0093	0.1065	0.0003	0.1452
25–30 MeV	-0.0010	0.0945	-0.0338	0.1485
30–50 MeV	-0.02943	0.0997	-0.0859	0.1603

Table 7.1: Comparison of energy resolution estimates for Michel electron ionisation energy.

the mean and RMS of the distribution. Table 7.1 gives a comparison between the estimated bias and resolution based on these two methods.

Contributions to Ionisation Energy Resolution

The ionisation energy resolution is made up of a combination of the hit–by–hit energy resolution, and the spread introduced due to imperfect hit tagging. The contribution from the hit–by–hit energy resolution can be estimated by considering the fractional energy difference in the case of perfect hit tagging, which sums up the reconstructed energy of all the true Michel electron hits in the image. The sum over the hits in each image is considered because this allows the error in the hit–by–hit recombination factor, which arises due to the use of an average recombination factor during reconstruction, to be averaged over the hits in the image. The fractional energy difference in this case is fit with a gaussian distribution, which is shown in Figure 7.22.

The contribution to the ionisation energy resolution due to the hit energy reconstruction was estimated based on the parameters from the gaussian fit in Figure 7.22. The bias in the hit energy reconstruction was estimated to be around 3%, and the resolution was estimated to be approximately 8%. The remaining energy resolution and bias seen in the Michel electron ionisation energy reconstruction is a result of the spread due to imperfect hit tagging.

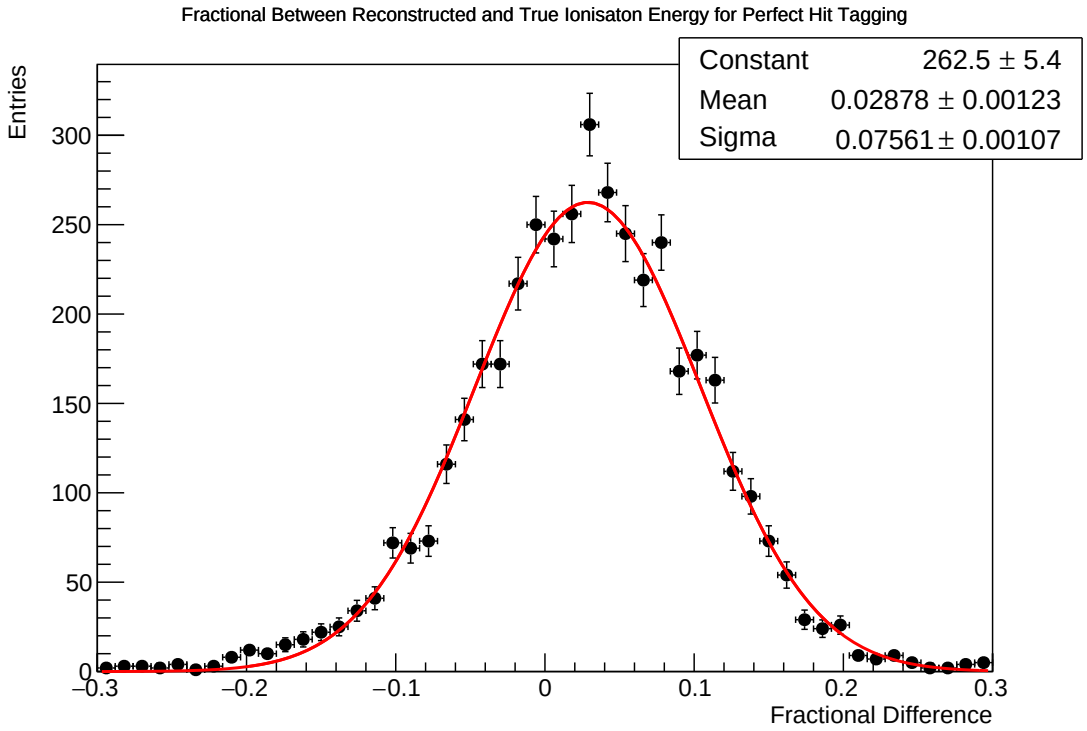

Figure 7.22: The fractional difference between the true ionisation energy deposition and the reconstructed ionisation energy deposition for Michel electron reconstructed with perfect hit tagging. The distribution is fit with a gaussian, which is shown in red, and the fit parameters are shown in the top right corner. The error bars are statistical.

Comparison to Other LArTPC Experiments

In order to put the performance of the Michel electron energy reconstruction into context, it is useful to compare the results presented here with those from other LArTPC experiments. We will restrict the comparisons here to the 0–30 MeV region for this comparison, recognising that improvements are still required in order to reduce the tail for higher energy ionisation energies. The closest comparison is against the MicroBooNE experiment, which is a surface level LArTPC which used ionisation energy for the reconstruction[121]. LArIAT and ICARUS have also performed Michel electron reconstruction[Amoruso:2003sw,Foreman$_2$016], *however*, $LArIATusedthescintillationlightforrecons$

The closest comparison for Michel electron energy reconstruction comes from the MicroBooNE LArTPC; both MicroBooNE and ProtoDUNE–SP are surface level TPCs, and they both use ionisation energy for Michel electron reconstruction. In MicroBooNE, the ionisation energy resolution for Michel electrons was found

to be between 15–25% in the 0–30 MeV region[121]. In this region the algorithm developed here gives an improved energy resolution of around 10%, which highlights the potential of the semantic segmentation approach if the bias at higher energies can be improved.

ICARUS also used ionisation energy for Michel electron reconstruction, however, the ICARUS detector was located deep underground, and therefore they were subject to much lower backgrounds. In ICARUS the ionisation energy resolution was measured to be in the range of 3–8%[122], however, these results did not take into account any radiated energy deposits, which form an important part of the Michel electron signature. Therefore, the results from ICARUS are not directly comparable to the measured energy resolution presented here.

LArIAT is a significantly smaller TPC than ProtoDUNE–SP, and therefore, despite being at surface level, there is a sufficiently low rate of cosmic rays that the photon detection system could be used to tag and measure Michel electron events. LArIAT measured an energy resolution on the order of 20% for Michel electrons based on the scintillation light signal[123].

In DUNE, both the ionisation energy and scintillation light will be used to reconstruct supernova neutrinos. The results in the DUNE Technical Design Report are based on energy resolution estimates from the standard LArSoft reconstruction framework, which give an ionisation energy resolution of around 20%, and a scintillation light energy resolution in the range of 10-20%[50]. Therefore, if the tail at high energy can be improved, a semantic segmentation algorithm, similar to the one presented here, may be able to improve the energy reconstruction performance for supernova neutrinos in the DUNE far detector. This is an important factor in many supernova neutrino physics studies, in which the mean neutrino energy is an important parameter[50].

7.4 Conclusion

In the energy regime of Michel electrons, and supernova neutrinos, the electromagnetic energy deposition of electrons moves from a ionisation dominated to a

radiation dominated region. As such, these events have a signature which contains both track–like and a shower–like components, and therefore they require a unique reconstruction algorithm in order to maximise the energy collected from the events.

In this chapter we have presented a novel Michel electron reconstruction algorithm based on machine learning techniques. A sample of Michel electrons was selected in ProtoDUNE–SP data with a purity of over 98% and an overall efficiency of around 5%. The ionisation energy of these events was reconstructed based on a semantic segmentation algorithm, which uses a U–Net CNN architecture. The performance of this algorithm shows an improvement in energy resolution over similar experiments, with an ionisation energy resolution of around 10-15%. However, there is still need for improvement, particularly in the high energy region where a large tail is seen in the fractional difference distribution.

The promising results in the low energy region based on this method, suggest that with further study the semantic segmentation approach could prove to be an effective algorithm for reconstructing low energy particles in LArTPCs. However, more work is required to ensure good performance across the desired energy range. In order to increase the performance in the high energy region, we could consider increasing the amount of training data in the high energy region. At the time of writing, there is insufficient ProtoDUNE–SP simulation to produce a flat training sample with sufficient data. Therefore, this remains as a possible future study into improving the performance of this algorithm.